Automated Segmentation of Computed Tomography Images

Justin Senseney[1], Paul F. Hemler[2], Matthew J. McAuliffe[1]
[1]BIRSS, Center for Information Technology, National Institutes of Health, Bethesda, MD 20892
[2]Dept. of Math and Computer Science, Hampden-Sydney College, Hampden-Sydney, VA 23943
senseneyj@mail.nih.gov, phemler@hsc.edu, mcmatt@exchange.nih.gov

Abstract

An image analysis, visualization, and segmentation system has been developed to assist researchers participating in a world-wide imaging study led by the National Institute on Aging to determine risk factors contributing to chronic osteoarthritis. The system provides a sophisticated but simple to use interface that directs the segmentation of muscle, fat, and other tissues of interest in thigh and abdomen computed tomography images.

1. Introduction

This paper describes a system to assist researchers and clinicians in segmentation and quantification tasks for the analysis of computed tomography (CT) images. This paper focuses on tools developed for use as a plug-in to the Medical Image Processing, Analysis, and Visualization (MIPAV) software program developed at the National Institutes of Health [5].

The developed system assists researchers participating in a National Institute on Aging led world-wide imaging study to determine risk factors contributing to chronic osteoarthritis. Accurate automated systems are required to assist researchers in evaluating the loss of muscle mass over a period of time [3]. Currently available manual systems do not provide the required analysis capabilities for conducting longitudinal studies relating to changes in body composition for a large cohort.

Body fat distribution measurement using CT images has previously led to significant observations in the study of osteoarthritis, obesity, and aging. Relative loss of muscle mass may become more important than measurements of body mass index (BMI) in determining health risks of obesity [11]. An increase of fat inside of muscle tissue is seen with an increase in age [10] [2], even though no significant change in BMI measurement occurs [1]. This research could use automated systems to allow larger data sets for quantifiable imaging studies. The system developed here provides an expandable interface to generate repeatable results and make larger longitudinal studies attainable.

As a computer-based medical system, successful implementation of this tool rests on an integrated understanding of its performance capabilities. A detailed description of the functionality presented in this paper, including the automated segmentation methods that have been derived from previous research and customized for the required tasks, are discussed. Customized semi-automatic tools, previously developed, are then reviewed.

Classification and quantification methods, including a brief overview of the user interface, are presented to aid understanding of this tool's role in the research framework. Finally, a comparative analysis of the automatic segmentation steps is presented along with ideas for future research directions.

2. Methods

The system automatically segments many of the desired tissues and provides advanced image processing tools to accurately and robustly assist technicians in semi-automatically determining the composition of the remaining, difficult to automatically segment muscles. Automatic segmentation techniques used in CT image analysis have been shown [12] to be useful tools for the applications presented herein. Although research into methods for automatic and semi-automatic methods have been well covered over the past fifteen years, few comprehensive systems exist to provide these methods directly to researchers interested in employing them in mass studies such as the osteoarthritis initiative.

The following sections describe the integrated methods that were developed by capitalizing on previous work in automatic computed tomography segmentation. These sections make use of the terms *right*, *left*, *top*, and *bottom* from the perspective of the observer to describe the work without regard to a particular orientation. The developed system is able to take an image's given orientation to develop segmented regions of interest which are labeled in a way that

appears anatomically correct to the research scientist.

2.1. Automatic Segmentation - Thigh

Past research has affirmed the intuition that image intensity plots of the lines in Figure 1 suggest that thresholding approaches to automatically segment the thigh, bone, and marrow are relatively straight forward [7]. Simple cases of the segmentation of the thighs, separated by air, are segmented using the following process. Equations 1 and 2 describe the segmentation process for the left thigh. The center of mass (*cm*) for the thresholded thigh c_l is determined by first separating the thresholded image I^* into left and right components I_l^* and I_r^*. This is done by finding an x^* near the center of the image where the points within a vertical line through I^* have intensity values of zero Hounsfield units. All points on either side of this line can then be grouped as part of either sub-image I_l^* or I_r^*.

$$I^* = threshold(750, 2000, I) \tag{1}$$

$$\begin{gathered} \exists x^* \, \forall y \;\; s.t. \;\; I^*(x^*, y) = 0 \\ I_l^* = I^*(x, y) \;\; \forall x < x^*, \;\; c_l = cm(I_l^*) \end{gathered} \tag{2}$$

With a center of mass from the thresholded image for each thigh we can perform the region growing (*rg*) covered in previous research. The parameter c_l derived in equation 2 is used as an initial seed point for this process. The seed point c_l or c_r is perturbed by δ_{ob} and δ_{ib} to be guaranteed outside the bone. δ_{ob} describes the top and left coordinates of the intersection of the outer-bone boundary with a vertical and horizontal line from c_l. δ_{ib} describes the bottom and right coordinates of this same intersection. Values between -300 and 900 Hounsfield units within the value of the marrow, *val*(c_l), in the original image *I* are included for *rg*.

$$rg\left(\begin{pmatrix} c_{l,x} + \delta_{ob,x} - \delta_{ib,x} \\ c_{l,y} + \delta_{ob,y} - \delta_{ib,y} \\ z \end{pmatrix}, val(c_l), -300, 900\right) \tag{3}$$

The process for segmenting connected thighs is considerably more difficult. Although previous research does address this topic from a generalized topology perspective, the following method proved to be advantageous. Let (δ_{ol}, δ_{or}) be a segment along the contour defined by the top portion of the thighs such that $\partial_x \delta_{ol} = \partial_x \delta_{or} = 0$. Let *r* be points along this segment of the contour.

$$\forall r \in (\delta_{ol}, \delta_{or}) \; \exists \{r^*\} \; s.t. \; \partial_x \left(\{r^*\}\right) \gg \partial_x(r) \tag{4}$$

$$\forall r \in \{r^*\} \; \exists r_t \; s.t. \; |r_{t,y}| > |r_y| \tag{5}$$

This process searches through the set of steep points r^* along the contour to find the minimum connecting point of the thighs r_t. This point has been found along the top portion of the thighs by finding the greatest absolute y-coordinate within the set r^*. The same process can be used to find the maximum connecting point along the contour defined by the bottom portion of the thighs.

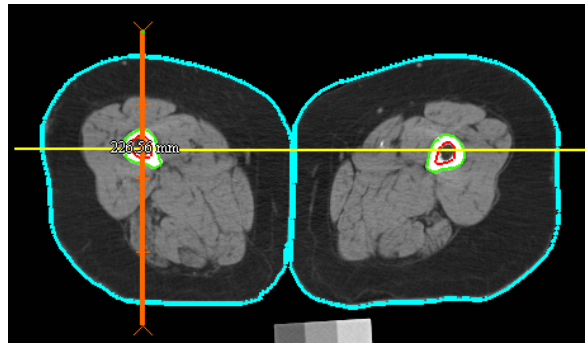

Figure 1. Connected thigh example.

The bone and marrow automatic segmentations prove to be fairly straightforward using previously developed threshold approaches [9]. Finally, quality control methods exist to avoid the creation of regions that are not useful approximations. Results for these automatic methods demonstrate that the system we have developed is useful for segmenting these images on a large scale. Quantitative results can be seen in section 4 Analysis.

Automatic segmentation of the requested muscle bundles proved infeasible. Partial voluming problems and other issues discussed in [7] demonstrate the difficulty of automatic muscle segmentation at a resolution finer than obtaining the overall muscle bundle. Semi-automatic methods exist for the segmentation of these muscles. Prior to a description of these methods, a summary of the automatic abdomen segmentation methods follows.

2.2. Automatic Segmentation - Abdomen

Automatic segmentation of the abdomen and subcutaneous fat in computed tomography images are described next. Image intensity profiles, of a given abdomen, suggest that region growing methods used in the automatic creation of thigh regions must be modified for segmentation of the subcutaneous area [12]. Methods for whole abdomen segmentation using region growing, thresholding, and error correction through iterative erosion/dilation proved to work well for most of the cases evaluated. Calcifications and voxel partial volume averaging make thigh segmentation a more complex problem.

For automatic abdomen segmentation, a seed point r^* is selected from the thresholded set *r'* that is as close to the origin as possible.

The seed point is guaranteed to be fat due to CT calibration. To remove possible partial voluming and bound-

ary noise errors near the skin boundary the seed point is perturbed a number of pixels δ_{sub} based on the nearest occurrence of muscle. A region growing (*rg*) process is performed using intensity values between -75 and 1500 Hounsfield units of the seed point's intensity.

$$rg\left(\begin{pmatrix} r^* + \delta_{sub,x} \\ r^* + \delta_{sub,y} \\ z \end{pmatrix}, val(r^* + \delta_{sub}), -75, 1500\right) \quad (6)$$

A morphological closing operation is performed to fill in gaps left by air pockets. These dilations and erosions are performed for up to ten iterations until only one object is identified within the abdomen area. *A* is the set of abdomen pixels/voxels, while *B* is the background image. As shown in Equation 7, the dilations and erosions occur using *A* and the complement of *B* to generate the automatically segmented abdomen area.

$$\bigcap_{\beta \in B^c} \left(\bigcup_{\beta \in B^c} (A + \beta) - \beta \right) \quad (7)$$

The subcutaneous area is automatically segmented using a revised algorithm of the one presented in [12]. This method works for both 2D and 3D images after prompting from the user.

Points referred to in this description may be seen on Figure 2. From the center of mass of a particular abdomen, radial trajectories are traversed in one degree increments to determine the location of the subcutaneous area. A particular trajectory first encounters multiple points of type *C* and *B* as it searches for the previously segmented abdomen. Once a trajectory encounters point *A*, point *B* is determined by traversing over possibly fat area until a muscle has been encountered. Each band is completed independently before deformable models and smoothing operations are performed. More information on deformable models can be found in the next section on semi-automatic methods.

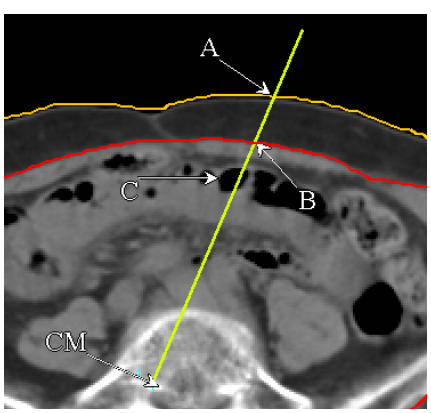

Figure 2. Subcutaneous fat segmentation.

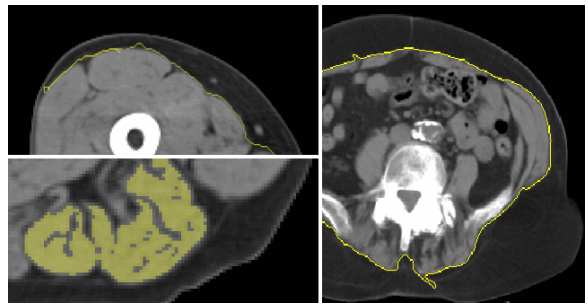

Figure 3. Clockwise from top-left; livewire example, level-set example, and region growing example images.

The segmentation of the abdominal muscles required for this study suffer from the same partial voluming problem preventing them from being automatically analyzed. The desired abdominal muscles include the psoas, lateral obliques, paraspinous, and rectus. The segmentation of the visceral cavity and calcium deposits located within the aorta are also required. This tool provides many semi-automatic methods, including Livewire [6], for segmenting the required muscles.

2.3. Semi-Automatic Segmentation

Livewire and level set methods are widely used tools for semi-automatic segmentation. The cost function of the livewire method is used to minimize the path traveled as a guide to a particular segmentation. When user-driven, this method draws two dimensional ROIs (Regions of Interest) initialized by a point defined by the cursor.

The static threshold option of region growing as used in this application is described by equations 8 and 9, given the image *I*, seed point r^*, and intensity constraints of *max* and *min*.

$$\forall r \in I \quad \delta < ||r^* - r||_\infty \quad \epsilon < ||r^* - r||_2 \quad (8)$$

$$\forall r' \in V_{\epsilon,\delta}(r) \; s.t. \; min \leq val(r') \leq max \quad (9)$$

The resulting set of *r'* is then the solution set of the region growing operation. This method is susceptible to unusual filling around the border of a desired object, as shown in the far right image in Figure 3. Such results are corrected using fuzzy connectedness methods [9].

3D CT images can be segmented on a single slice and then propagated to other slices using the software's custom propagation buttons. These buttons attempt to evolve a given VOI by the approximate derivatives given by a b-spline approximation to the contour.

Each of these semi-automatic methods are complimentary to the automated methods discussed and have also been

shown to be essential in segmenting the muscles from computed tomography images within the more general framework.

3. Classification and Quantification

The segmentation tool's user interface is an extension of the main MIPAV interface. All of the tools available in MIPAV can be used in this system, and in some cases have been customized. Filters, morphological operations, VOI identifiers, look up table operations, and painting/VOI creation methods that aid in the eventual classification and quantification of tissue are available through the MIPAV interface.

The design and implementation of classification and quantification methods in this system supports custom operations as required. The user interface can be changed through a graphical custom segmentation builder to support a larger variety of computed tomography datasets than the ones presented here. This custom interface can then be saved to a locally defined preferences file. Previously created VOIs are automatically loaded into the custom interface. By allowing the researcher to select which muscles or other parts of the body should be considered within this tool, the custom interface allows the tool to be used for user-defined classification and quantification tasks.

3.1. Tissue Classification

Threshold classification of CT images allows identification of muscle and fat tissue within the thigh and abdomen. Partial voluming effects are decreased by adopting a schema found in recent literature [7].

$-190 \leq$ fat pixel ≤ -30

$0 \leq$ muscle pixel ≤ 100

$-30 <$ partial volume pixel < 0

This classification system can be assigned to a lookup table (LUT). Applying the given LUT to a CT abdomen image yields the result shown in Figure 4.

The partial voluming effects are denoted by white pixels in this figure. These pixels fall in the range of -30 to 0 Hounsfield units. Such pixels are counted as part of a particular muscle's total tissue area/volume when they fall under a given VOI. However, such pixels are not counted as part of a given VOIs total muscle or intramuscular fat area/volume. Implications of this counting method are discussed in the results section.

3.2. Muscle and Fat Quantification

Muscle and interstitial fat are identified using the tissue intensity values previously discussed. Pixels are then categorized by the VOI that contains them and aggregated to yield reports such as the one in Figure 5.

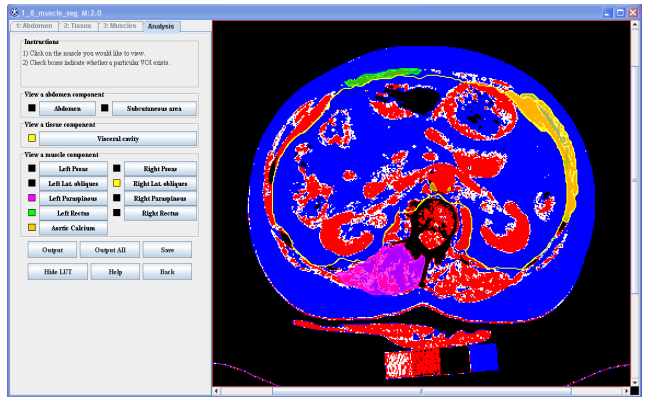

Figure 4. Custom look up table applied to a partially segmented abdomen.

This segmentation tool calculates the total fat, lean, and aggregate area in any particular VOI and also computes the mean Hounsfield unit for each of these sets. In cases where multiple curves exist (such as liver cysts) the total area is the compilation of all created curves.

The PDF report seen in Figure 5 is automatically created using the open source and freely available program iText [4]. The MIPAV statistics generator has also been customized for this tool to produce total fat, lean, and aggregate areas for each VOI (Volume of Interest) in addition to the statistics already available, such as the center of mass, eccentricity, and major or minor axis length. The output generated from these tools can be imported into an analysis program for further evaluation.

3.3. Customization

Derivations of the presented classification and quantification tasks are possible through an interface designed to allow this system to be used for other research projects that involve computed tomography images. The abdomen and thigh tools presented here generate local preference files in a modifiable format. This allows researchers to specify muscles or other tissues of interest to a particular project.

Interface modifications can be made either manually or within the system, generating a new set of saved preferences that can be selected later. These modifications are presented to the researcher as custom created objects that are present in all parts of the research framework. Intestinal obstructions, unusual calcifications, or specific muscle bundles are examples of objects that can be added through this interface. These objects can then be included in relevant calculations and displayed appropriately. Items of interest that are added in this way can be included in the automatically generated PDF report such as the one shown in Figure 5.

Sample	UCSD	MIPAV	% Diff
5937	173.760	174.2	0.25
5942	180.363	180.4	0.02
6331	173.782	173.3	-0.28
6332	190.564	190.8	0.12
6336	242.377	242.5	0.05
6338	191.921	194.3	1.24
6385	220.804	220.9	0.04
6464	170.393	170.7	0.18
6516	148.458	148.6	0.10
6518	235.119	236.6	0.63
6577	153.155	153.2	0.03
6593	259.180	259.1	-0.03
6597	182.600	182.5	-0.05
Average % Difference			0.18
Standard Deviation			0.38

Table 1. Left thigh measurement comparison. All measurements in cm^2.

Sample	UCSD	MIPAV	% Diff
5937	177.047	177.3	0.14
5942	178.775	179.3	0.29
6331	173.036	173.6	0.33
6332	188.736	189.3	0.30
6336	253.816	253.8	-0.01
6338	204.483	208.0	1.72
6385	229.073	229.7	0.27
6464	178.967	179.3	0.19
6516	150.194	150.6	0.27
6518	241.165	239.0	-0.90
6577	157.35	157.6	0.16
6593	253.172	253.0	-0.07
6597	195.246	196.0	0.39
Average % Difference			0.24
Standard Deviation			0.55

Table 2. Right thigh measurement comparison. All measurements in cm^2.

Researcher defined tissues of interest can also affect the calculations of other objects. For example, a researcher may not want to include identified calcifications in the quantification of muscle mass. These calcifications can be assigned a location within the developed system and assigned a flag that indicates calculations should be performed. The relevant calcification calculations will then be removed from a given muscle's values for area, volume, and mean Hounsfield units. No customization was made for the analysis presented in the next section.

4. Analysis

Preliminary results from this tool were compared to a segmented dataset from the University of California, San Diego (UCSD). The UCSD data were composed of 13 thigh and 13 abdomen CT scans that were later segmented using our tool. The freehand segmentations were generated and processed using a program developed at UCSD. This program computed the areas, subject to the same partial voluming errors encountered within the MIPAV based tool, and then printed the areas in a PDF report.

4.1. Thigh Results

All 13 of the two dimensional thigh CT scans processed by our tool yielded successful automatic segmentations of the thigh, bone and marrow for both the left and right thigh. Our generated area of the thigh was then directly compared to the UCSD's manually segmented data values for the thigh after subtracting area values for the bone and marrow.

As can be seen in tables 1 and 2, the UCSD and our segmentations had an average percent difference of .18 percent in the left thigh and .24 percent in the right thigh. Compared to the average percentage difference, the comparatively large standard deviation suggests two important facts. First, a larger sample of previously segmented data should be used before useful generalizations can be made about the effectiveness of the automatic segmentations. Second, it reminds one that in any computer-based medical system, a manual inspection of automatically generated data, VOIs in this case, is needed before the data is used to draw any significant conclusions. Still the small average percent difference between the UCSD and MIPAV produced areas suggests that this tool presents a useful innovation when encountering a project where the manual demands of segmenting an image would be too laborious and subjective.

4.2. Abdomen Results

The same comparison of 13 datasets from UCSD was used to compare automatic segmentation of the abdomen and subcutaneous fat with the previous manual segmentation. In this case a higher standard deviation, though still low average percent difference of 1.12 percent was encountered from automatic segmentation of the abdomen as shown in Table 3. The standard deviation suggests that on average, our tool is overextending the definition of abdomen tissue to phantoms that may exist in the image. As with segmentation of the thigh, the average percent difference may still be small enough that this tool would be a useful asset in a large scale project such as the osteoarthritis initiative at the National Institute on Aging.

Sample	UCSD	MIPAV	% Diff
5937	384.366	391.7	1.91
5942	564.618	580.3	2.78
6331	145.039	133.9	-7.68
6332	411.284	424.2	3.14
6336	419.321	429.9	2.52
6338	340.017	343.9	1.14
6385	454.456	468.9	3.18
6464	411.451	425.2	3.34
6516	331.362	337.1	1.73
6518	418.129	427.4	2.22
6577	309.173	306.9	-0.74
6593	488.844	489.2	0.07
6597	384.320	388.1	0.98
Average % Difference			1.12
Standard Deviation			2.92

Table 3. Abdomen measurement comparison. All measurements in cm^2.

Automatic segmentation of the subcutaneous area encountered similar problems to those from attempting to segment the fascia border in the thigh case. This suggests semi-automatic segmentation tools are useful in optimizing the results of the subcutaneous segmentation. Without such an optimization the average percent difference of the subcutaneous fat area and mean Hounsfield unit from the automatic segmentation are presented in Table 4. The average percent difference of the Hounsfield unit is only about half as large as the average percent difference for the subcutaneous fat. These percentages present either an area of further refinement for our tool or the need for manual inspection of the automatically generated VOIs to ensure the integrity of results. The segmentation of subcutaneous fat in these abdominal images is a further step in the evolution of the method originally proposed in [12].

5. Conclusion

The software package described in this paper provides robust and novel methods for segmentation and analysis of computed tomography thigh and abdomen images in both two and three dimensions. By leveraging MIPAV's existing utilities with custom operations, a tool has been developed which proves advantageous to existing software methods for faster, reliable, and repeatable segmentation and analysis of CT images.

Further development into automatic and semi-automatic segmentation methods to enhance the algorithms developed for a greater complexity of images is necessary. The software provides a useful framework for testing new image processing algorithms and functionality.

	% Diff	Std Dev
Abdomen Fat	2.34	1.92
Subcutaneous Fat	3.06	3.58
Subcutaneous Fat HU	1.57	1.50

Table 4. Resulting percentage differences for the subcutaneous fat, accompanying Hounsfield unit, and total abdomen fat.

Analysis of the developed automatic segmentations can also be further improved. Comparisons made here to the manually segmented UCSD data set indicate that this segmentation program generates adequate results when compared to a segmentation program that has previously been used for active research. Further analysis would compare the segmentation efforts of this program to accessible clinical measurements to determine the general reliability and accuracy of this program.

Testing is critical to ensure the reliability of the automatically generated results. The testing presented in this paper indicates that our system provides invariant, accurate results across a spectrum of computed tomography images. The segmentation process using this system is faster than existing manual segmentation systems. This system provides robust segmentation and calculation abilities that with further work will make large scale studies such as the world-wide osteoarthritis initiative feasible.

5.1. Acknowledgments

This work was supported by the Intramural Research Program of the National Institutes of Health and the Center for Information Technology at the National Institutes of Health.

References

[1] K. F. Adams, A. Schatzkin, T. B. Harris, V. Kipnis, T. Mouw, R. Ballard-Barbash, A. Hollenbeck, and M. F. Leitzmann. Overweight, obesity, and mortality in a large prospective cohort of persons 50 to 71 years old. *New England Journal of Medicine*, 355(8):763–778, 2006.

[2] A. E. Field, E. H. Coakley, A. Must, J. L. Spadano, N. Laird, W. H. Dietz, E. Rimm, and G. A. Colditz. Impact of overweight on the risk of developing common chronic diseases during a 10-year period. *Archives of Internal Medicine*, 161(13):1581–1586, 2001.

[3] B. Goodpaster, S. Park, and T. B. Harris. The loss of skeletal muscle strength, mass, and quality in older adults: The health, aging and body composition study. *The Journal of Gerontology: Medical Sciences*, 61A(10):1059–1064, 2006.

[4] B. Lowagie. *iText in Action: Creating and Manipulating PDF*. Manning, New York, 2006.

[5] M. McAuliffe, F. Lalonde, D. McGarry, W. Gandler, K. Csaky, and B. Trus. Medical image processing, analysis and visualization in clinical research. In *Computer-Based Medical Systems, 2001. CBMS 2001. Proceedings. 14th IEEE Symposium on*, pages 381–386, 2001.

[6] E. Mortensen and W. Barrett. Interactive segmentation with intelligent scissors. *Graphical Models and Image Processing*, 60(5), 2001.

[7] S. Ohshima, S. Yamamoto, T. Yamaji, M. Suzuki, M. Mutoh, M. Iwasaki, S. Sasazuki, K. Kotera, S. Tsugane, Y. Muramatsu, and N. Moriyama. Development of an automated 3d segmentation program for volume quantification of body fat distribution using ct. *Japanese Journal of Radiological Technology*, 64(9):1177–1181, 2008.

[8] D. Pham and J. Prince. Adaptive fuzzy segmentation of magnetic resonance images. *IEEE Transactions on Medical Imaging*, 18(9):737–752, 1999.

[9] J. Udupa and S. Samarase. Fuzzy connectedness and object definition: Theory algorithms and applications in image segmentation. *Graphical Models and Image Processing*, 58(3), 1996.

[10] M. Zamboni, F. Armellini, T. B. Harris, E. Turcato, R. Micciolo, I. Bergamo-Andreis, and O. Bosello. Effects of age on body fat distribution and cardiovascular risk factors in women. *American Journal of Clinical Nutrition*, 66(1):111–115, 1997.

[11] M. Zamboni, G. Mazzali, E. Zoico, T. B. Harris, J. Meigs, V. Francesco, F. Fanti, L. Bissoli, and O. Bosello. Health consequences of obesity in the elderly: a review of four unresolved questions. *International Journal of Obesity*, 29:1011–1029, 2005.

[12] B. Zhao, J. Colville, J. Kalaigian, S. Curren, J. Li, P. Kijewski, and L. Schwartz. Automated quantification of body fat distribution on volumetric computed tomography. *Journal of Computer Assisted Tomography*, 30(5), 2006.

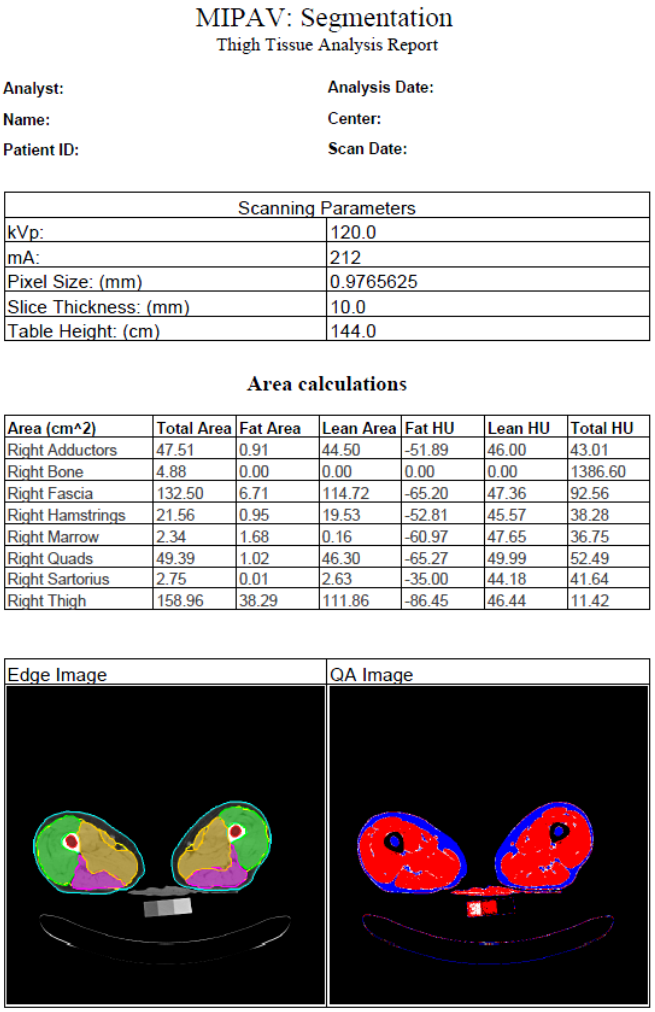

MIPAV: Segmentation

Thigh Tissue Analysis Report

Analyst: **Analysis Date:**

Name: **Center:**

Patient ID: **Scan Date:**

Scanning Parameters	
kVp:	120.0
mA:	212
Pixel Size: (mm)	0.9765625
Slice Thickness: (mm)	10.0
Table Height: (cm)	144.0

Area calculations

Area (cm^2)	Total Area	Fat Area	Lean Area	Fat HU	Lean HU	Total HU
Right Adductors	47.51	0.91	44.50	-51.89	46.00	43.01
Right Bone	4.88	0.00	0.00	0.00	0.00	1386.60
Right Fascia	132.50	6.71	114.72	-65.20	47.36	92.56
Right Hamstrings	21.56	0.95	19.53	-52.81	45.57	38.28
Right Marrow	2.34	1.68	0.16	-60.97	47.65	36.75
Right Quads	49.39	1.02	46.30	-65.27	49.99	52.49
Right Sartorius	2.75	0.01	2.63	-35.00	44.18	41.64
Right Thigh	158.96	38.29	111.86	-86.45	46.44	11.42

Edge Image QA Image

Figure 5. Automatically generated PDF file containing relevant calculations for a two dimensional thigh image.